

Recent Results from the H1 Experiment at HERA

Armen Buniatyan*

Physics Institute of University of Heidelberg

E-mail: Armen.Buniatyan@desy.de

On behalf of the H1 Collaboration

A review is presented of recent results from the H1 Experiment at the electron-proton collider HERA. The summary comprises new results on the quark and gluon structure of the proton, on the strong coupling α_s , on the production of jets and hadrons and on hard diffractive scattering.

The XXI International Workshop High Energy Physics and Quantum Field Theory

June 23 - 30, 2013

Saint Petersburg Area, Russia

*Speaker.

1. Introduction

The HERA was the worlds only electron-proton collider, operated during the years 1992 to 2007. It was producing ep interactions at centre-of-mass energies up to $\sqrt{s} = 320$ GeV. Two collider experiments, H1 and ZEUS, collected data corresponding to an integrated luminosity of 0.5 fb^{-1} each.

The HERA collider was an unique machine for studying strong interactions. It provided a clean environment for the precise determination of the proton structure over a wide range of Bjorken x and virtuality Q^2 of the exchanged boson, which is either a photon or a Z -boson in case of neutral current (NC) interaction, $ep \rightarrow eX$, or a W -boson in case of charged current (CC) interaction $ep \rightarrow \nu X$. The high resolution multi-purpose detectors H1 and ZEUS allow for detailed analyses of hadronic final state and thereby give access to the vast physics of diffraction and of jet, heavy quark and particle production. By all these processes different aspects of strong interactions are addressed making HERA an ideal testing ground for quantum chromodynamics (QCD). In this talk the recent results of H1 Experiment are reviewed, in particular of the measurement of inclusive DIS cross sections, the hadronic final states and the hard diffractive processes.

2. Inclusive DIS cross sections at high Q^2

A precise knowledge of the proton parton distribution functions (PDFs) is vital for interpreting the data taken at hadron colliders, especially when analysing rare Standard Model, SM , processes or when searching for signs of new physics. All modern proton PDFs are based on the proton structure function data from HERA. At HERA, the structure of the proton was probed with electrons and positrons. Figure 1 illustrates a diagram of deep inelastic scattering, DIS .

Inclusive ep DIS NC and CC cross section measurements may be used to determine the combined sea quark distribution functions and the valence quark distributions in the proton. A QCD analysis in the DGLAP formalism also allows the gluon momentum distribution in the proton to be determined from scaling violations. The NC (and similarly CC) cross section can be expressed in terms of structure functions:

$$\frac{d^2\sigma_{NC}^{e^{\pm}p}}{dx dQ^2} = \frac{2\pi\alpha^2}{xQ^4} [Y_+ \tilde{F}_2^{\pm} \mp Y_- x\tilde{F}_3^{\pm} - y^2 \tilde{F}_L^{\pm}],$$

where $Y_{\pm} = 1 \pm (1-y)^2$ with y being the inelasticity. The structure function \tilde{F}_2 is the dominant contribution to the cross section. $x\tilde{F}_3$ is important at high Q^2 and \tilde{F}_L is sizable only at high y . In the framework of perturbative QCD ($pQCD$) the structure functions are directly related to the parton distribution functions, i.e. in leading order (LO) F_2 is the momentum sum of quark and anti-quark distributions, $F_2 \approx x \sum e_q^2 (q + \bar{q})$, $x\tilde{F}_3$ is related to their difference $x\tilde{F}_3 \approx x \sum 2e_q a_q (q - \bar{q})$. At higher orders, terms related to the gluon density distribution ($\alpha_s g$) appear.

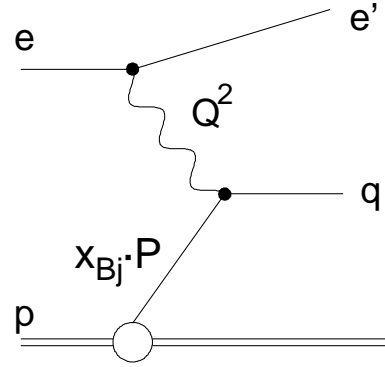


Figure 1: Feynman diagram of deep inelastic lepton-proton scattering

Recently, H1 collaboration has finalised the inclusive cross section measurements at high Q^2 with HERA-II data [1]. Inclusive ep cross sections for NC and CC DIS scattering processes measured with the H1 detector are in the range of Q^2 between 60 and 50.000 GeV² and Bjorken x between 0.0008 and 0.65. The measurements are performed for 4 distinct data sets which correspond to the data taken with either the electron (e^-) or the positron (e^+) lepton beams with either left handed (L) and right handed (R) polarisation. Polarisation is defined as $P_e = (N_R - N_L)/(N_R + N_L)$, where N_R (N_L) is the number of right (left) handed leptons in the beam. The luminosity and longitudinal lepton beam polarisation for each data set are given in table 1.

	R	L
$e^- p$	$\mathcal{L} = 47.3 \text{ pb}^{-1}$ $P_e = (+36.0 \pm 1.0)\%$	$\mathcal{L} = 104.4 \text{ pb}^{-1}$ $P_e = (-25.8 \pm 0.7)\%$
$e^+ p$	$\mathcal{L} = 101.3 \text{ pb}^{-1}$ $P_e = (+32.5 \pm 0.7)\%$	$\mathcal{L} = 80.7 \text{ pb}^{-1}$ $P_e = (-37.0 \pm 0.7)\%$

Table 1: Table of integrated luminosities, \mathcal{L} , and luminosity weighted longitudinal lepton beam polarisation, P_e , for the data sets presented here.

To obtain unpolarised cross section measurements, the left and right handed $e^\pm p$ samples were combined into unpolarised data sets. The measurements are combined with earlier published HERA-1 H1 data [2]-[4]. In the left side of Figure 2 the double differential reduced NC cross section is presented as a function of x and Q^2 . The reduced cross section is defined as

$$\tilde{\sigma}_{NC}(x, Q^2) = \left[\frac{d^2 \sigma_{e^\pm p}^{NC}}{dx dQ^2} \right] / \left[\frac{2\pi\alpha^2 Y_\pm}{xQ^4} \right]$$

The Q^2 dependence of the unpolarised NC and CC cross sections is shown in the right side of Figure 2. At low Q^2 the NC cross section is larger than the CC cross section by two orders of magnitude. Approaching the mass of the Z and W bosons, the cross sections of NC and CC processes become of the same magnitude, demonstrating an *unification* of the electroweak interactions at high Q^2 .

In this analysis an ultimate precision of 1.5-2% for NC and up to 4% for CC measurements is reached. This allows for a determination of proton PDFs with much improved precision. The PDFs are determined from all published NC and CC H1 data. The fitting is performed using the HERAFitter [5], which is an open source QCD fit framework designed for the extraction of PDFs and the fast assessment of the impact of the new data. The parton distributions as a function of x at $Q^2 = 10 \text{ GeV}^2$, determined from the NLO QCD fit to the H1 NC and CC data, denoted as ‘H1PDF 2012’, are shown in Figure 3. Significant improvement of precision compared to the previous PDF fits is reached for all parton distributions. In Figure 2 the Standard Model expectation which use the H1PDF 2012 parameterisations are compared to the NC and CC cross sections. The data distributions are well described by the SM predictions.

The total CC cross section, σ_{CC}^{tot} , was measured as an integrated cross section in the kinematic region $Q^2 > 400 \text{ GeV}^2$ and $y < 0.9$ for the $e^- p$ and $e^+ p$ data and for different longitudinal lepton beam polarisations. The cross sections are shown in the left side of Figure 4 together with the unpolarised data from HERA-1 and the SM expectations using H1PDF 2012 parameterisation. Also

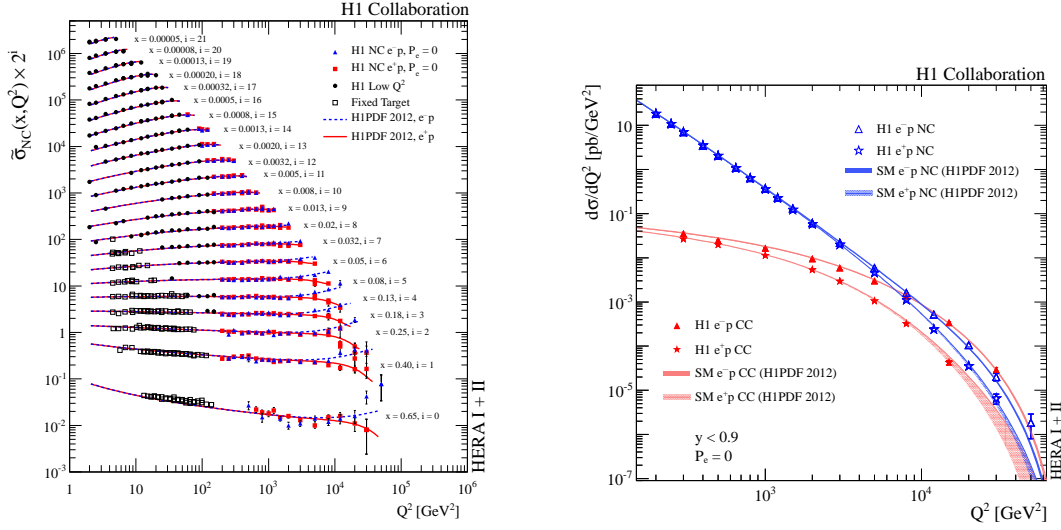


Figure 2: Right: the Q^2 dependence of the unpolarised $e^\pm p$ NC and CC cross sections compared to the SM expectation from H1PDF 2012 proton PDF parameterisation.

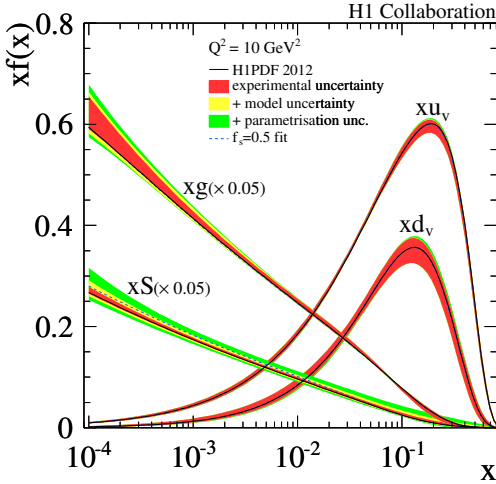


Figure 3: Parton distribution functions of H1PDF 2012 at the evolved scale of 10 GeV^2 . The uncertainties include the experimental uncertainties (inner), the model uncertainties (middle) and the parametrisation variation (outer).

shown are the linear fits to the polarisation dependence of the measured cross sections simultaneously to $e^- p$ and $e^+ p$ data. The SM predicts a polarisation dependence of total CC cross section of the form: $\sigma_{CC}^\pm(P_e) = (1 \pm P_e)\sigma_{CC}^\pm(0)$. The extrapolation of the cross section with the fit to the point $P_e = +1$ for $e^- p$ and $P_e = -1$ for $e^+ p$ excludes the existence of a right handed W^R boson of mass M_W^R below 214 GeV (194 GeV for $e^+ p$) at 95% confidence level, assuming SM couplings and a light right handed ν_e . This textbook measurement demonstrates the absence of right handed weak current.

In the SM the difference in the NC DIS cross sections for leptons with different helicity states is predicted due to chiral structure of the neutral electroweak exchange. The NC parity violating structure function $F_2^{\gamma Z}$ can be determined from these cross sections as

$$F_2^{\gamma Z} \sim [\sigma^-(P_L) - \sigma^-(P_R)] - [\sigma^+(P_L) - \sigma^+(P_R)]$$

In the right side of Figure 4 the first measurement of the γZ interference structure functions is

presented. It is well described by the SM, using H1PDF 2012 parameterisation.

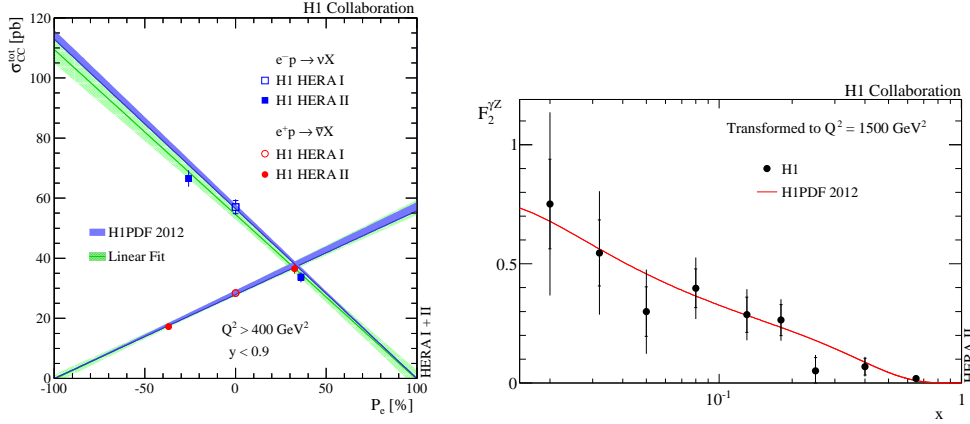


Figure 4: Left: the dependence of the $e^\pm p$ CC cross section on the lepton beam polarisation P_e in comparison with the SM prediction and the linear fit of the polarisation dependence. Right: the γZ interference structure function $F_2^{\gamma Z}$. Both measurements are compared to the Standard Model predictions based on the H1PDF 2012 parameterisation

3. Charged particle spectra in DIS

The DIS processes at HERA give access to small values of Bjorken x at low four momentum transfer squared Q^2 of a few GeV^2 . In the region of low x , characterised by high densities of gluons and sea quarks in the proton, the parton interaction with the virtual photon may originate from a cascade of partons emitted prior to the interaction. In QCD such multi-parton emissions are described only within certain approximations valid in restricted phase space regions. Measurements of the transverse momentum spectra of charged particles allow testing of different approaches for parton evolution dynamics. In addition, such measurement serve as a test for various phenomenological models. Here two recent H1 measurements of charged particle production in DIS are discussed. The analyses are based on data collected with the H1 detector at ep centre-of-mass energies of $\sqrt{s} = 319\text{GeV}$ [6] and $\sqrt{s} = 225\text{ GeV}$ [7].

Several mechanisms contribute to hadron production. At low transverse momenta, p_T , the production of hadrons is dominated by the hadronisation effects, while at higher p_T the parton dynamics effects dominate. Monte Carlo (MC) generators, which use different approaches to simulate the parton cascade, are compared to the measurements: RAPGAP [8] based on leading log DGLAP parton showers; DJANGO [9] based on Colour Dipole Model (CDM), as implemented in ARIADNE [10], with a description of parton emission similar to that of the BFKL evolution; CASCADE [11] based on the CCFM model, which unifies the BFKL and DGLAP approaches and requires angular ordering of the emitted partons. In the CDM and the CCFM approaches the p_T of the emitted partons in a parton shower is not ordered in x . All generators use the Lund string model [12] for hadronisation with parameters tuned by the ALEPH collaboration to fit LEP data [13].

The p_T dependence of charged particle densities at $\sqrt{s} = 319\text{ GeV}$ is studied in two pseudo-rapidity intervals, $0 < \eta^* < 1.5$ and $1.5 < \eta^* < 5$, referred to as the "central region" and "current

region", respectively. Such division separates the regions of sensitivity to the hard scattering process (current region), from the region of parton showering (central region). The measurement at reduced proton beam energies ($\sqrt{s} = 225$ GeV) allows for a more precise measurement of the "central region". Therefore for this analysis the p_T spectra are measured in seven bins in the pseudorapidity region $0 < \eta^* < 3.5$.

The charged particle densities as a function of pseudorapidity are shown in Figure 5 for two different regions in p_T^* . The different fragmentation models are compared to the measurements. Details in the fragmentation process mainly influence the low p_T^* -region while the large p_T^* region is rather insensitive to fragmentation. The same particle densities are shown in Figure 6 in comparison with the MC models using different parton evolution mechanisms. Here, the low p_T^* -region shows only little dependence on the parton cascade while the differences due to parton showering are clearly visible at large p_T^* . Best description at all p_T^* is provided by DJANGO (CDM) model. The CASCADE MC fails in describing the data in both regions.

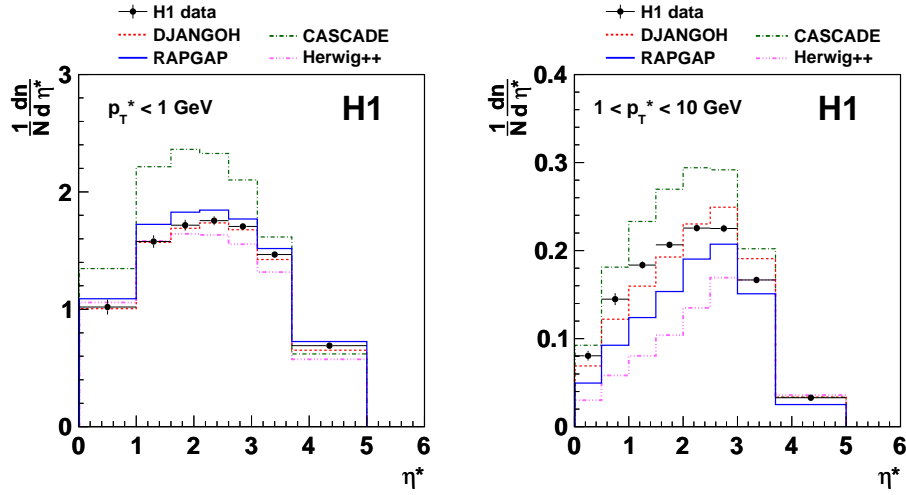


Figure 5: Charge particle densities as function of pseudorapidity measured for $p_T^* < 1$ GeV and $1 < p_T^* < 10$ GeV regions. The MC predictions using different hadronisation models are compared to the measurement.

The transverse momentum spectra p_T^* of charged particles are presented in Figure 7. DJANGO describes the data fairly well for the whole p_T^* range, whereas RAPGAP is significantly below the data for $p_T^* > 1$ GeV. CASCADE is above the data for almost the whole p_T^* range.

The data taken at reduced proton beam energy $E_p = 460$ GeV ($\sqrt{s} = 225$ GeV) allows us to achieve better acceptance and resolution in the central rapidity region. The ratios of MC predictions to the data are shown in Figure 8 as a function of p_T^* . Both models, RAPGAP and DJANGO, fail to describe the data.

4. Very forward neutron and photon production in DIS

Measurements of particle production at very small angles with respect to the proton beam direction (forward direction) in ep collision are important for the understanding of proton fragmentation. Measurements of forward particle also provide important constraints for modelling of

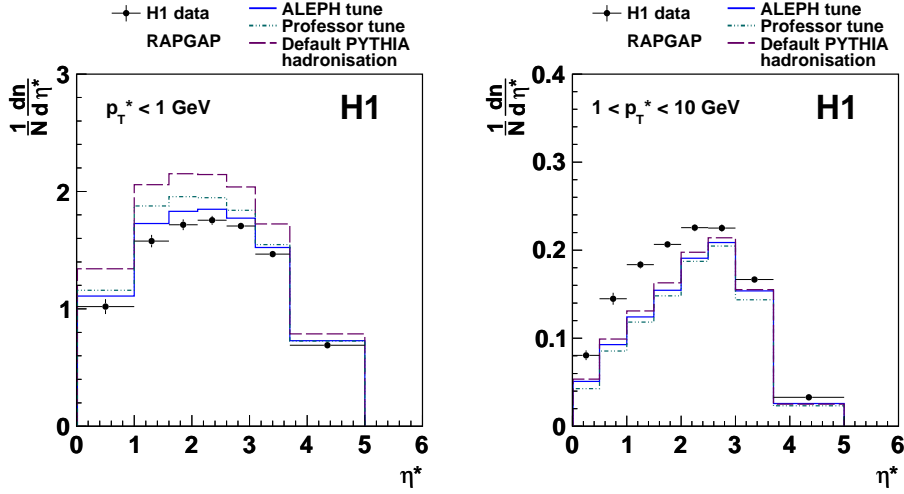


Figure 6: Charge particle densities as function of pseudorapidity measured for $p_T^* < 1$ GeV and $1 < p_T^* < 10$ GeV regions. The MC predictions using different parton evolution models are compared to the measurement.

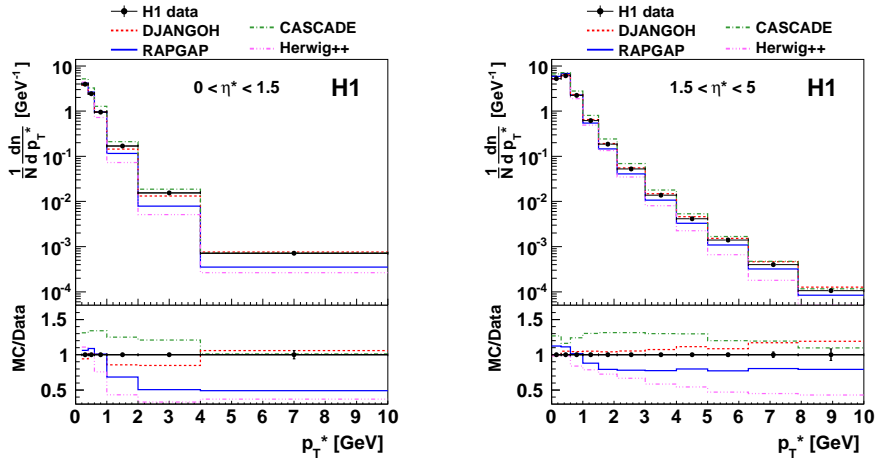


Figure 7: The measured transverse momentum spectra of charged particles together with different MC prediction and the ratios MC over data shown for central and current regions respectively.

high energy air showers and thereby are very valuable for the understanding of high energy cosmic ray data.

New results from the H1 Experiment on very forward photon and neutron production in deep-inelastic positron-proton scattering (DIS) are reported [14]. The photons and neutrons are measured in the Forward Neutron Calorimeter (FNC) [15, 16], which was installed at 106 m from the ep interaction point at a polar angle 0° with respect to the proton beam direction at the interaction point. The acceptance of the FNC is defined by the aperture of the HERA beam-line magnets and is limited to scattering angles of $\theta < 0.8$ mrad or pseudorapidity $\eta > 7.9$.

Differential cross sections normalised to the inclusive DIS cross sections are measured for for-

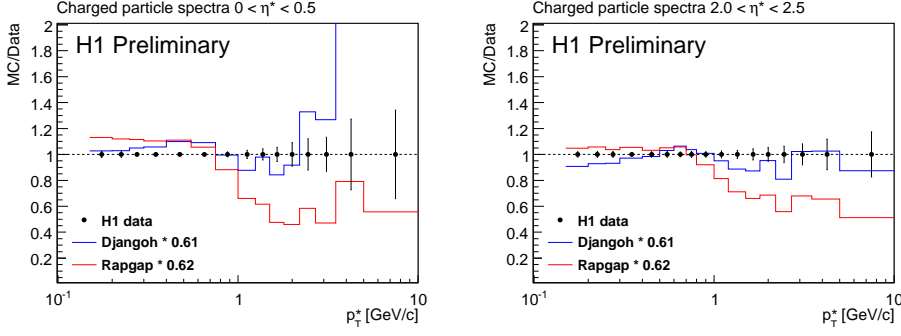


Figure 8: Ratios of MC over data for charged particle p_T^* spectra measured at $\sqrt{s} = 225$ GeV shown for central and current regions, respectively.

ward photons and neutrons as a function of the Feynman- x variable $x_F = p_{||}^*/p_{||max}^*$ for three ranges of virtual photon-proton centre-of-mass energy, W : $70 < W < 130$ GeV, $130 < W < 190$ GeV and $190 < W < 250$ GeV. The measurements are shown in Figures 9 and 10 together with the MC model predictions. The DJANGO program is used to generate inclusive DIS events. Higher order QCD effects are simulated using leading log parton showers as implemented in LEPTO [17], or using the Colour Dipole Model (CDM). In addition the RAPGAP pion-exchange model is used to describe the high x_F part of forward neutron spectra.

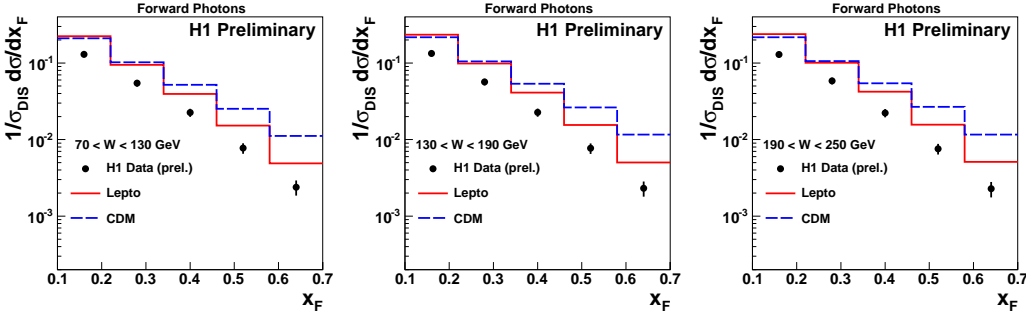


Figure 9: Normalised cross sections for forward photon production as a function of x_F compared to predictions of the LEPTO and CDM MC models.

In Figure 9 the cross sections measured for the most energetic photons with pseudorapidity $\eta > 7.9$ is shown as a function of Feynman x variable for three W region compared to CDM or LEPTO MC models. Both models significantly overestimate the rate of forward photons by $\sim 70\%$. The shape of the LEPTO prediction is close to the data, while CDM exhibits a harder x_F behaviour.

The measured normalised x_F distributions for forward neutron production are presented in Figure 10. The predictions of MC models CDM, RAPGAP- π (pion-exchange) and their combination using weighting factors obtained from the fit to the neutron energy distribution are compared to the measurement. The combination model describes the data well.

The data are also compared with Cosmic Ray (CR) hadronic interaction models commonly used for the simulation of CR air shower cascades: EPOS [18], QGSJET 01 [19] [20], QGSJET II [21, 22] and SIBYLL [23, 24]. The comparison of the CR hadronic interaction model predic-

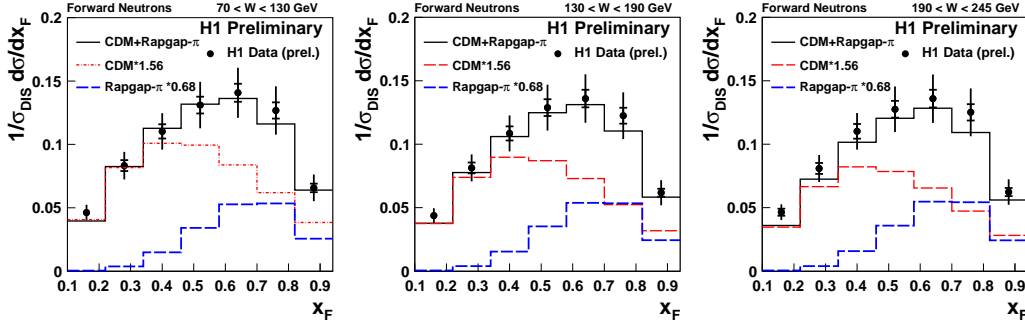


Figure 10: Normalised cross sections for forward neutron production as a function of x_F compared to predictions of the CDM and RAPGAP- π MC models and their combination.

tions with the data is shown in Figure 11 for one range of W . A large difference between the model predictions is observed. None of the models can describe the forward photon and neutron measurements simultaneously.

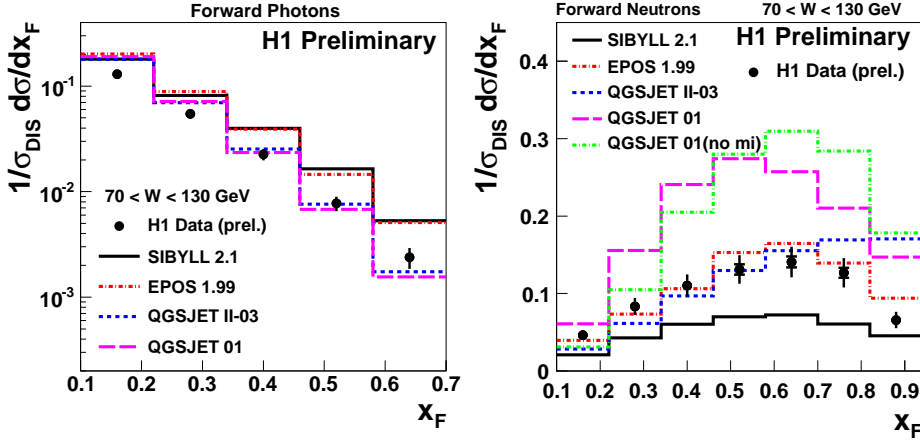


Figure 11: Normalised cross sections for forward photon and neutron production as a function of x_F compared to predictions of the Cosmic Ray hadronic interaction models.

5. Multijet production in DIS

The strong coupling, α_s , is the fundamental parameter of perturbative QCD (pQCD). The running of α_s is predicted by the pQCD. The absolute normalisation, however, must be determined by experiment. The H1 and ZEUS Collaborations performed extensive studies of the jet production processes in the different kinematic regimes. These measurements allowed the determinations of α_s at HERA with an unprecedented level of precision.

In ep collisions at HERA one distinguishes two processes according to the virtuality Q^2 of the exchanged boson, the Deep Inelastic Scattering (DIS) and photoproduction. In DIS a highly virtual boson ($Q^2 > 1 \text{ GeV}^2$) interacts with a parton carrying a momentum fraction of the proton. In photoproduction a quasi-real photon ($Q^2 < 1 \text{ GeV}^2$) interacts with a parton from the proton either directly or via its constituent. In the pQCD, a jet cross section is expressed as the convolution of

the parton distribution functions (PDFs) in the proton (and in the photon for the photoproduction) with the matrix elements. In regions where the PDFs are well constrained, the jet data allow testing of the general aspects of pQCD. In regions where the PDFs are not so well constrained, jet cross sections can be incorporated into global QCD fits, which would lead to the reduction of the PDF uncertainties.

Jet production in ep collisions proceeds via the Born, boson-gluon fusion and QCD Compton processes. In the Breit frame, where the virtual boson and the proton collide head on, the significant transverse momenta P_T are produced at leading order (LO) in α_s by the boson-gluon fusion and QCD Compton processes. Jet production with P_T in the Breit frame is thus directly sensitive to α_s . In the analyses presented here the jets are defined using the k_T clustering algorithm, which is applied in the Breit frame for DIS and in the photon-proton collinear frame for photoproduction. The associated cross sections are collinear and infrared safe and therefore are well suited for comparison with the predictions from the fixed order QCD calculations.

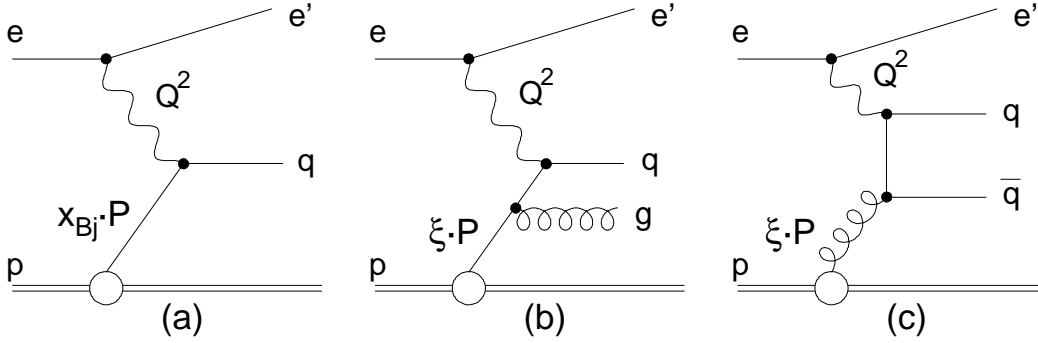


Figure 12: Deep-inelastic lepton-proton scattering at different orders in α_s : (a) Born contribution $\mathcal{O}(1)$ and $\mathcal{O}(\alpha_s)$ processes (b) QCD Compton scattering and (c) boson-gluon fusion.

The H1 Collaboration reported new measurement [25] of inclusive jet, 2-jet and 3-jet production at high Q^2 Neutral Current (NC) DIS ($150 < Q^2 < 15000 \text{ GeV}^2$). The measured differential cross sections as a function of transverse momenta of the jets $P_{T,jet}$ (or the average transverse momentum of two or three leading jets $\langle P_T \rangle_{jet}$ in the 2-jet and 3-jet events) in the regions of Q^2 normalised to the inclusive DIS cross section are shown in the left side of Figure 13. For this measurement the ultimate 1% jet energy scale uncertainty is achieved.

The NLO QCD calculations provide a good description of the jet measurements, both in the DIS and the photoproduction regimes. The NLO QCD fitting technique is applied to these measurements in order to extract the strong coupling α_s . The values $\alpha_s(M_Z) = 0.1163 \pm 0.0011(\text{exp.}) \pm 0.0014(\text{PDF}) \pm 0.0008(\text{had.}) \pm 0.0039(\text{theory})$ for H1 DIS jet measurement is obtained. The value of $\alpha_s(M_Z)$ from this measurement is shown in the right side of Figure 13 together with the values from other HERA measurements and world average [26]. Within uncertainties, which are dominated by the uncertainties of theory calculations due to missing higher orders, the obtained values of α_s agree with each other and with the world average.

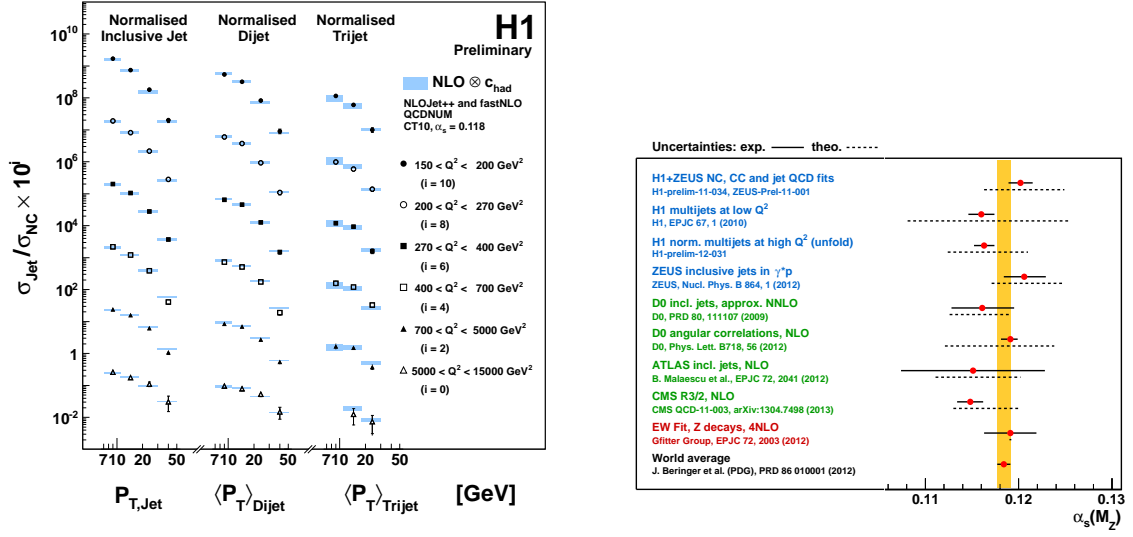


Figure 13: (Left) the inclusive jet, dijet and trijet production cross sections in DIS normalised to the DIS cross section as a function of jet transverse momentum in the Breit frame $P_{T,jet}$ or the average transverse momentum of two or three leading jets $P_{T,jet}$, measured in the regions of Q^2 . The NLO QCD calculations, corrected for hadronisation effects are compared to the measurements. (Right) values of $\alpha_s(M_Z)$ obtained from the HERA data and other measurements.

6. Diffraction at HERA

6.1 Measurement of Inclusive Diffractive DIS

About 10% of the DIS cross section measured at low Bjorken x at HERA are due to diffractive processes, such as $ep \rightarrow eXp$. Diffractive DIS can be viewed as process in which the virtual photon probes a net colour singlet combination of exchanged partons. In processes of diffractive production of jets and heavy vector mesons, the P_T of the jet and the mass of heavy quark provide a hard scale for perturbative calculations.

The diffractive interactions at HERA are identified employing two different methods: by requirement of the absence of hadronic activity in the direction of proton (*large rapidity gap* or LRG method) or by a direct measurement of scattered proton in the dedicated forward proton spectrometers (*leading proton* or FPS method). The accuracy of the LRG method is limited by the systematics related to the missing leading proton and by the contribution from the proton dissociation, while the FPS method is limited by low acceptance of proton spectrometers and by the proton tagging systematics.

In Figure 14 the diffractive reduced cross section $\sigma_r^{D(3)}$ from H1 as measured by the LRG method based on the full HERA statistics [27] is compared with the pQCD predictions using the diffractive parton distribution functions (DPDFs) H1 2006 Fit B set [28]. The data are well described for $Q^2 > 10 \text{ GeV}^2$. Also shown are the FPS measurement from H1 [30], scaled by a factor 1.2, which accounts for the contribution of proton dissociation to the LRG data. The cross section measurements agree well with each other

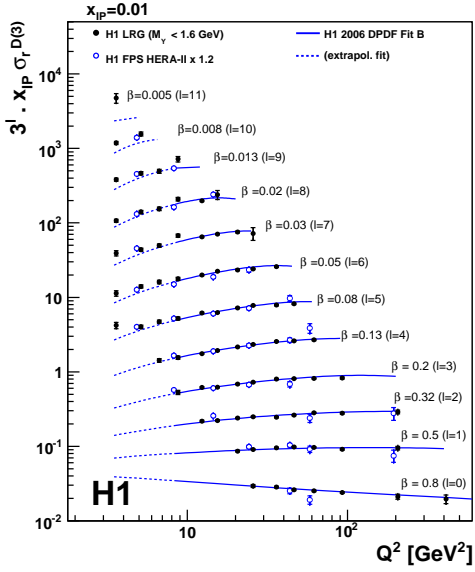


Figure 14: Reduced diffractive cross section from combined H1 LRG data $x_P \sigma_r^{D(3)}$ at $x_P = 0.01$. The LRG data are compared with the H1 FPS results ⁷

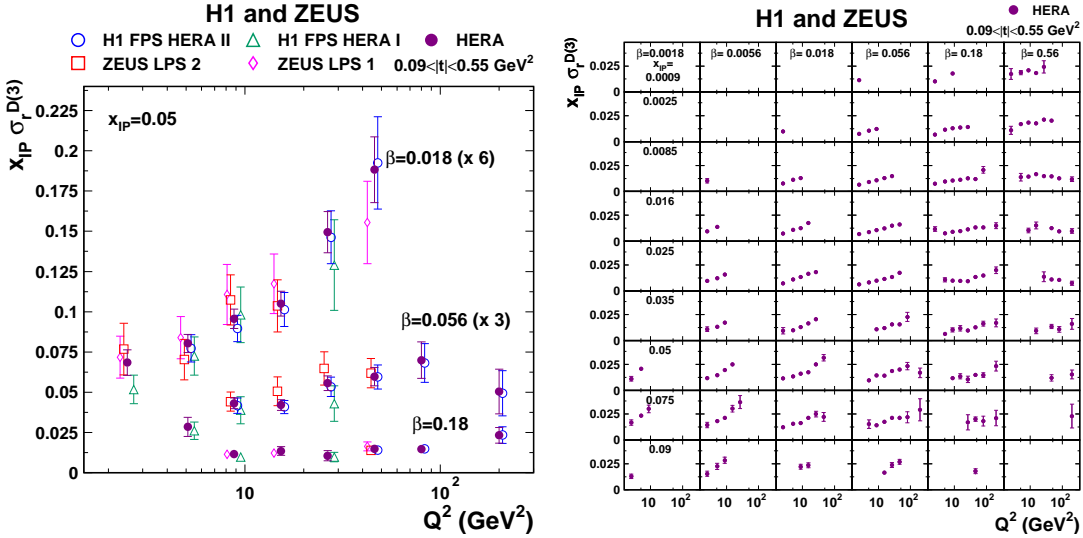


Figure 15: Reduced diffractive cross section $x_P \sigma_r^{D(3)}(\beta, Q^2, x_P)$ for $0.09 < |t| < 0.55 \text{ GeV}^2$ as a function of Q^2 for different values of β at $x_P = 0.05$. The combined data are compared to the H1 and ZEUS data input to the averaging procedure.

The H1 and ZEUS Collaborations performed the combination of the diffractive DIS cross sections [30, 31, 32, 33] measured using their proton spectrometers in the range $0.09 < |t| < 0.55 \text{ GeV}^2$ in squared four-momentum transfer at the proton vertex [34]. The H1 and ZEUS diffractive DIS cross sections are combined using χ^2 minimisation procedure [29]. The result of the combination is shown in Figure 15. In the left side figure also the uncombined data are shown in one x_P bin. Due to the cross calibration of the correlated systematic uncertainties of both experiments the combined data are more precise than each measurement alone. The cross sections indicate strong rise with Q^2 , which implies the scaling violation and large contribution from the gluons to the diffractive interactions.

6.2 Diffractive jet photoproduction with a leading proton

According to the QCD factorisation theorem [35], the parton distribution functions extracted from the QCD fits to diffractive structure functions can be used to describe hadronic final states in diffractive DIS. The universality of these diffractive parton distribution functions (DPDFs) was experimentally confirmed in DIS regime for different processes, such as jet, charm and vector meson production. However, in diffractive hadron-hadron interactions the theoretical predictions which use DPDF from the HERA inclusive DIS measurements overestimate the data [36, 37]. The effect is usually explained as a consequence of additional partonic interactions between the hadrons which destroy the rapidity gap [38].

In ep interactions at HERA, if the electron scatters at very small angles and Q^2 is very small, the virtual photon can be considered to be almost real. In these interactions, which are referred to as ‘*photoproduction*’, in the LO approximation the photon may fluctuate into a long-lived partonic state. Then only a part of photon four-momentum [participates in the hard interaction. Such interactions are called resolved photon interactions. The resolved photon interactions resemble the hadron-hadron interactions. The photon can also couple directly to the quarks, and these interactions are called direct photon interactions. The variable x_γ , which is defined as a four-momentum fraction of the photon which participates in the hard interaction, is used to distinguish between the direct and resolved photon processes. For direct processes $x_\gamma = 1$, while for resolved processes $x_\gamma < 1$.

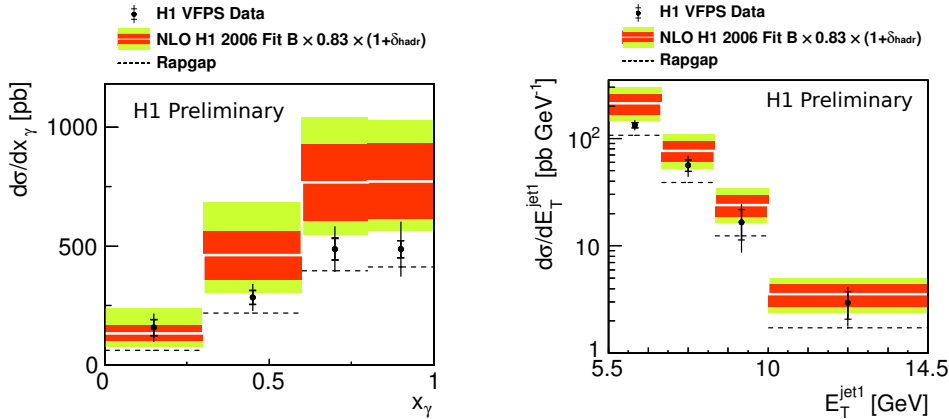


Figure 16: The differential cross section for the diffractive photoproduction of dijets, with the leading proton measured in the H1 very forward proton spectrometer VFPS. The NLO calculations are compared to the measurements.

In diffractive processes, due to analogy of resolved photon with hadron-hadron interactions, one might expect similar effects leading to the breaking of rapidity gap [39, 40]. In the previous H1 and ZEUS analyses [41, 42, 43] the diffractive events were selected by a large rapidity gap method, and contrary to the theoretical expectations, no significant dependence of data suppression factor on x_γ is observed. The H1 observed a breaking of factorisation by an overall suppression factor of about 0.6 with respect to the NLO QCD predictions, while ZEUS data are compatible with no factorisation breaking hypothesis. Here a new measurement of this process by the H1 Experiment is presented [44]. The analysis uses the data collected in 2006-2007, and the diffractive events are

selected by tagging a forward proton in a very forward proton spectrometer (VFPS) located at 220-222 m from the interaction point down the beampipe in proton direction. This method profits from the fact that the measurement is free of contribution from proton dissociation and non-diffractive processes. The events with two jets of energies $E_T^{jet1} > 5.5$ GeV and $E_T^{jet2} > 4$ GeV are selected in the central detector using the k_T algorithm. The final data sample corresponding to the kinematic range $Q^2 < 2$ GeV², $0.010 < x_p < 0.024$ and $|t| < 0.6$ GeV² contains about 4800 events. The data were unfolded to hadron level using singular value decomposition of the response matrix [45].

The measured differential cross sections as a function of x_γ and E_T^{jet1} are shown in Figure 16. The NLO QCD prediction overestimate the measurements by

$$\sigma_{DATA}/\sigma_{NLO} = 0.67 \pm 0.04(stat.) \pm 0.09(sys.) \pm 0.20(scale) \pm 0.14(DPDF).$$

No obvious dependence of a suppression factor on x_γ is observed. The result is consistent with previous H1 result [42].

6.3 Exclusive Heavy Vector Meson (VM) Photoproduction

The H1 Collaboration performed a simultaneous measurement of J/ψ photoproduction in elastic and proton dissociation processes [46]. The measurement results are based on two data sets: the data taken in the years 2006 - 2007, when HERA was operated with proton beam energy 920 GeV, resulting in $\sqrt{s} \approx 318$ GeV, corresponding to an integrated luminosity of 130 pb⁻¹ and the data recorded in 2007 before the final HERA shutdown, when the proton beam energy was reduced to 460 GeV, resulting in $\sqrt{s} = 225$ GeV, corresponding to an integrated luminosity of 10.8 pb⁻¹. The J/ψ mesons are reconstructed in the $J/\psi \rightarrow \mu^+\mu^-$ and e^+e^- decay channels. A diagram for a diffractive J/ψ -meson production and the invariant mass distributions are shown in Figure 17.

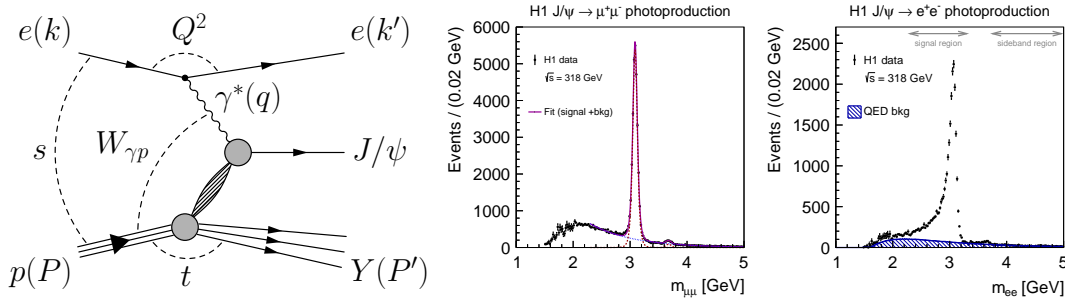


Figure 17: A diagram for Diffractive J/ψ production in ep collision and the dilepton invariant mass distributions in the $J/\psi \rightarrow \mu^+\mu^-$ and $J/\psi \rightarrow e^+e^-$ decay channels.

Regularised unfolding is used to determine the elastic and proton-dissociative cross section in bins of t and $W_{\gamma p}$. The measured elastic and proton-dissociative cross sections differential in $|t|$ are shown in Figure 18. The cross sections fall steeply as a function of $|t|$, with a clear difference between the shapes of the proton-dissociative and elastic distributions. The elastic and proton-dissociative differential cross sections $d\sigma/dt$ are fitted simultaneously. The elastic cross section is parametrised as $d\sigma/dt = N_e e^{-b_e|t|}$. For the proton-dissociative cross section the parametrisation $d\sigma/dt = N_{pd}(1 + (b_{pd}/n)|t|)^{-n}$ is chosen, which interpolates between an exponential at low $|t|$ and a power law behaviour at high values of $|t|$. The obtained parameterisations for the elastic and

proton-dissociative cross sections are compared to the data in Figure 18. The elastic cross section data for $|t| > 0.1$ GeV are well described by the exponential parametrisation. The fall of elastic cross section with increasing $|t|$ is much faster than the proton-dissociative cross section, which is reflected in the values for b_{el} and b_{pd} : $b_{el} = (4.88 \pm 0.15)\text{GeV}^{-2}$ and $b_{pd} = (1.79 \pm 0.12)\text{GeV}^{-2}$.

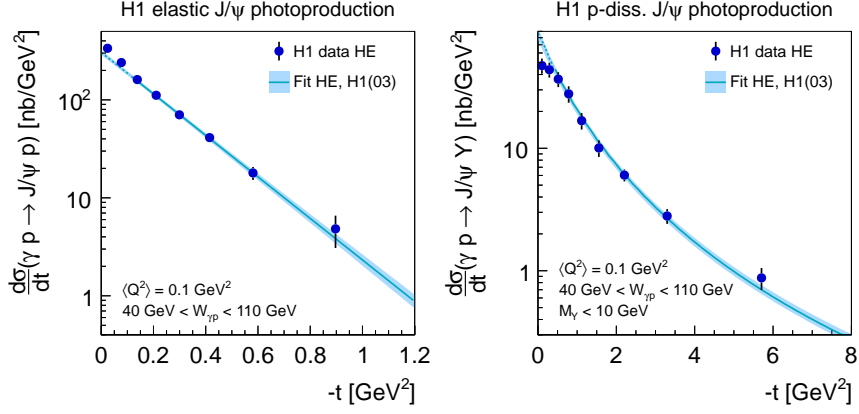


Figure 18: Differential J/ψ photoproduction cross section $d\sigma/dt$ as function of the negative squared four-momentum transfer at the proton vertex $-t$, as obtained for elastic and proton-dissociative regimes.

The measured elastic and proton-dissociative cross sections as a function of $W_{\gamma p}$ are shown in Figure 19. The elastic and proton-dissociative cross sections are of similar size at the lowest $W_{\gamma p} = 30$ GeV accessed in this analysis. The elastic cross section rises faster with increasing $W_{\gamma p}$ than the proton-dissociative one. Also shown is the ratio of the proton-dissociative to the elastic cross section as a function of $W_{\gamma p}$. The ratio decreases from 1 to 0.8 as $W_{\gamma p}$ increases from 30 GeV to 100 GeV. The elastic and the proton-dissociative cross sections as a function of $W_{\gamma p}$ are fitted simultaneously, taking into account the correlations between these cross sections. As parametrisation a power law function of the form $\sigma = N(W_{\gamma p}/W_{\gamma p,0})^\delta$ with $W_{\gamma p,0} = 90$ GeV is used, with separate sets of parameters for the elastic and the proton-dissociative cases. The result of the fit is compared to the measurements. The fit results to the values $\delta^{el} = 0.67 \pm 0.03$ and $\delta^{pd} = 0.42 \pm 0.05$.

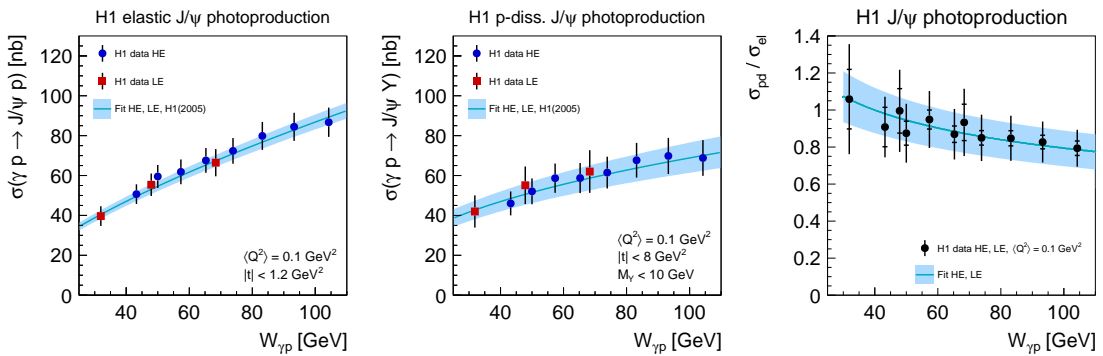


Figure 19: J/ψ photoproduction cross section as function of photon proton centre-of-mass energy $W_{\gamma p}$ for the elastic and proton-dissociative regime. The rightmost figure shows the ratio of the elastic to the proton-dissociative J/ψ photoproduction cross section as a function of $W_{\gamma p}$.

A compilation of cross section measurements for the elastic J/ψ photoproduction cross section is shown in Figure 20 as a function of $W_{\gamma p}$. The data from the present analysis fall in the gap between the data of fixed target experiments [49, 50] at low $W_{\gamma p}$ and the bulk of the previous high $W_{\gamma p}$ HERA data. The fixed target data exhibit a lower normalisation and a steeper slope than observed at HERA. Also shown are recent results from the LHCb experiment [51]. The extrapolated fit function for the H1 elastic J/ψ photoproduction cross section describes the LHCb data points at high $W_{\gamma p}$ well.

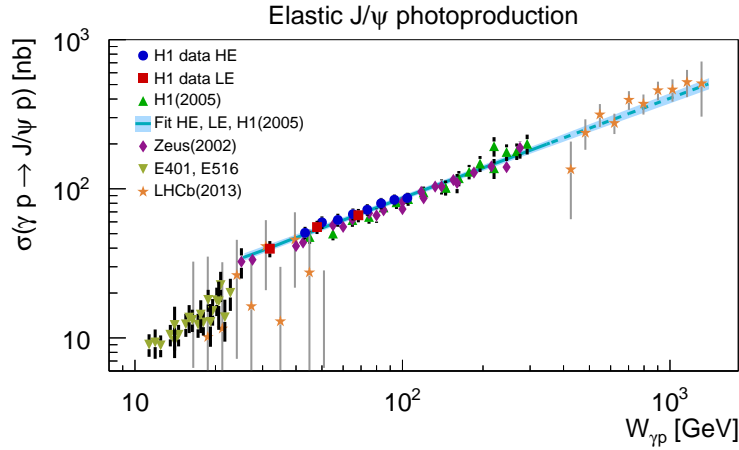


Figure 20: Compilation of various elastic J/ψ photoproduction cross section measurements including this measurement, previous HERA results [47, 48], results from fixed target experiments [49, 50] and from the LHCb [51] experiment.

7. Conclusions

Six years after the end of data taking, H1 is an active experiment producing valuable results in a broad area of particle physics. Presented here is a subjective selection taken from the wealth of new measurements of deep inelastic scattering, production of jets and hadrons and diffractive interactions. Much progress has been made over recent years, in the type of studies that can be performed, the precision achieved and in theoretical understanding. The final analyses of the full data samples significantly improve our understanding of the QCD and the proton structure.

Acknowledgements

I would like to thank organisers for this interesting, stimulating and enjoyable conference.

References

References

- [1] H1 Collaboration, F. D. Aaron et al., *JHEP* **1209**, 061 (2012) [arXiv:1206.7007].
- [2] H1 Collaboration, C. Adloff et al., *Eur. Phys. J. C* **13**, 609 (2000) [hep-ex/9908059].
- [3] H1 Collaboration, C. Adloff et al., *Eur. Phys. J. C* **19**, 269 (2001) [hep-ex/0012052].
- [4] H1 Collaboration, C. Adloff et al., *Eur. Phys. J. C* **30**, 269 (2003) [hep-ex/0304003].

- [5] HERAFitter, <http://herafitter.org>
- [6] H1 Collaboration, C. Alexa et al., *Eur. Phys. J. C* **73**, 2406 (2013) [arXiv:1302.1321].
- [7] H1 Collaboration, “Measurement of charged particle production in deep-inelastic ep scattering at $\sqrt{s} = 225$ GeV at HERA”, H1prelim-13-032
<http://www-h1.desy.de/h1/www/publications/htmlsplit/H1prelim-13-032.long.html>
- [8] H. Jung, *Comput. Phys. Commun.* **86** (1995) 147.
- [9] K. Charchula, G. A. Schuler and H. Spiesberger, *Comput. Phys. Commun.* **81** (1994) 381.
- [10] L. Lönnblad, ARIADNE 4.10, *Comput. Phys. Commun.* **71** (1992) 15.
- [11] H. Jung, *Comput. Phys. Commun.* **143** (2002) 100 [hep-ph/0109102].
- [12] T. Sjöstrand, *Comput. Phys. Commun.* **39** (1986) 347.
- [13] ALEPH Collaboration, S. Schael et al., *Phys. Lett. B* **606**, 265 (2005).
- [14] H1 Collaboration, “Analysis of Feynman scaling of Photon and Neutron Production in the Very Forward Direction in Deep-Inelastic Scattering at HERA”, H1prelim-13-012
<http://www-h1.desy.de/h1/www/publications/htmlsplit/H1prelim-13-012.long.html>
- [15] H1 Collaboration, F.D. Aaron et al., *Eur. Phys. J. C* **71**, 1771 (2011) [arxiv:1106.5944].
- [16] H1 Collaboration, F.D. Aaron et al., *Eur. Phys. J. C* **68**, 381 (2010) [arxiv:1001.0532].
- [17] G. Ingelman, A. Edin and J. Rathsman, LEPTO 6.5, *Comput. Phys. Commun.* **101** (1997) 108 [hep-ph/9605286].
- [18] K. Werner, F.-M. Liu and T. Pierog, *Phys. Rev. C* **74**, 044902 (2006) [hep-ph/0506232].
- [19] N.N. Kalmykov and S.S. Ostapchenko, *Phys. Atom. Nucl.* **56** (1993) 346.
- [20] N.N. Kalmykov, S.S. Ostapchenko and A.I. Pavlov, *Nucl. Phys. Proc. Suppl.* **52B** (1997) 17.
- [21] S.S. Ostapchenko, *Phys. Rev. D* **74**, 014026 (2006) [hep-ph/0505259].
- [22] S.S. Ostapchenko, *AIP Conf. Proc.* **928**, 118 (2007) [arXiv:0706.3784].
- [23] J. Engel et al., *Phys. Rev. D* **46**, 5013 (1992).
- [24] E.-J. Ahn et al., *Phys. Rev. D* **80**, 094003 (2009) [arXiv:0906.4113].
- [25] H1 Collaboration, “Normalised Multi-jet Cross Sections using Regularised Unfolding and Extractions of $\alpha_s(M_Z)$ in DIS at high Q^2 at HERA”, H1prelim-12-031,
<https://www-h1.desy.de/h1/www/publications/htmlsplit/H1prelim-12-031.long.html>.
- [26] S. Bethke, *Nucl. Phys. B. (Proc. Suppl.)* **222-224** (2012) 94.
- [27] H1 Collaboration, F.D. Aaron et al., *Eur. Phys. J. C* **72**, 2074 (2012).
- [28] H1 Collaboration, A. Aktas et al., *Eur. Phys. J. C* **48**, 715 (2006) [hep-ex/0606004].
- [29] A. Glazov, *AIP Conf. Proc.* **792** (2005) 237.
- [30] H1 Collaboration, A. Aaron et al., *Eur. Phys. J. C* **71**, 1578 (2011) [arxiv:1010.1476].
- [31] H1 Collaboration, F.D. Aaron et al., *Eur. Phys. J. C* **48**, 749 (2006) [hep-ex/0606003].
- [32] ZEUS Collaboration, S. Chekanov et al., *Eur. Phys. J. C* **38**, 43 (2004).
- [33] ZEUS Collaboration, S. Chekanov et al., *Nucl. Phys. B* **816**, 1 (2009).

- [34] H1 and ZEUS Collaborations, F.D. Aaron et al., *Eur. Phys. J. C* **72**, 2175 (2012) [arxiv:1207.4864].
- [35] J.C. Collins, *Phys. Rev. D* **57**, 3051 (1998), *Phys. Rev. D* **61**, 019902 (2000).
- [36] CDF Collaboration, A.A. Affolder et al., *Phys. Rev. Lett.* **84**, 5043 (2000).
- [37] CMS Collaboration, S. Chatrchyan et al., *Phys. Rev. D* **87**, 012006 (2013) [arXiv:1209.1805].
- [38] J. Bjorken, *Phys. Rev. D* **47**, 101 (1993).
- [39] A. Kaidalov, V. Khose, A. Martin and M. Ryskin, *Phys. Lett. B* **567**, 61 (2003) [hep-ph/0306134].
- [40] A. Kaidalov, V. Khose, A. Martin and M. Ryskin, *Phys. Lett. B* **559**, 235 (2003) [hep-ph/0302091].
- [41] H1 Collaboration, A. Aktas et al., *Eur. Phys. J. C* **51**, 549 (2007) [hep-ex/0703022].
- [42] H1 Collaboration, F. Aaron et al., *Eur. Phys. J. C* **70**, 15 (2010) [arXiv:1006.0946].
- [43] ZEUS Collaboration, S. Chekanov et al., *Eur. Phys. J. C* **55**, 177 (2008) [arXiv:0710.1498].
- [44] H1 Collaboration, H1prelim-13-011,
<https://www-h1.desy.de/h1/www/publications/htmlsplit/H1prelim-13-011.long.html>
- [45] A. Hocker and V. Kartvelishvili, *Nucl. Instr. Meth.* **A372** (1996) 469-481 [hep-ph/9509307].
- [46] H1 Collaboration, C. Alexa et al., *Eur. Phys. J. C* **73**, 2466 (2013) [arxiv:1304.5162].
- [47] H1 Collaboration, A. Aktas et al., *Eur. Phys. J. C* **46**, 585 (2006) [hep-ex/0510016].
- [48] ZEUS Collaboration, S. Chekanov et al., *Eur. Phys. J. C* **24**, 345 (2002) [hep-ex/0201043].
- [49] M. E. Binkley et al., *Phys. Rev. Lett.* **48**, 73 (1982).
- [50] B. H. Denby et al., *Phys. Rev. Lett.* **52**, 795 (1984).
- [51] LHCb Collaboration, R. Aaij et al., *J. Phys. G* **40** (2013) 045001 [arXiv:1301.7084].